

Porosity in plasma electrolytic oxide coatings

J.A. Curran, T.W. Clyne *

Department of Materials Science and Metallurgy, Cambridge University, Pembroke Street, Cambridge CB2 3QZ, UK

Received 9 August 2005; received in revised form 27 November 2005; accepted 16 December 2005

Available online 28 February 2006

Abstract

Plasma electrolytic oxide coatings are generally assumed to be almost fully dense. However, evidence is presented here for the presence of sub-micrometre, surface-connected porosity in such coatings, on aluminium alloys, at levels of the order of 20%. This evidence comes from densitometry, mercury porosimetry, helium pycnometry, BET adsorption measurements and high-resolution scanning electron microscopy. The very fine scale of the porosity (pore diameter ~ 10 to 100 nm), coupled with severe difficulties in making unambiguous microstructural observations, may account for the failure to detect this feature previously. It is pointed out that various measured properties, such as Young's modulus and thermal conductivity, are consistent with the presence of these relatively high porosity levels. Various other observed characteristics can also be explained on this basis. Finally, a possible mechanistic origin for the porosity is proposed. © 2006 Published by Elsevier Ltd on behalf of Acta Materialia Inc.

Keywords: Coating; Crystalline oxides

1. Introduction

Plasma electrolytic oxide (PEO) coatings [1–4] (sometimes referred to as micro-arc oxide coatings, or spark/discharge anodic coatings) are formed by substrate oxidation in an aqueous electrolyte via a series of localised electrical discharge events. These discharges allow oxide growth to proceed so as to produce films with thicknesses of the order of 100 μm . They are being explored and developed for various applications, including those for which wear resistance [5–10], corrosion resistance [7,9,11] and thermal protection [12–14] are being sought. Among the attractions of the process are that it involves very few health or safety hazards, and that coatings of uniform thickness can be quickly and easily produced on components with complex surface geometry, over a wide range of sizes.

However, much remains to be established before these coatings can be efficiently exploited and find widespread use. In particular, despite extensive study of the deposition process [15–18] and of coating microstructures [19–21], the

mechanism of coating growth remains somewhat unclear, particularly in terms of the local physical processes occurring during growth. The coating structure also remains rather poorly characterised.

The present paper is focused on the porosity and pore architecture exhibited by PEO coatings. There has been very little previous work aimed specifically at this area, although it has generally been stated and assumed that the porosity level is low. Figures of the order of a few per cent have commonly been quoted, with the assumption often made that this is largely associated with the deep pipe-like structures left by the most recent discharge events. However, there have been very few previous attempts at quantitative measurement of the porosity content of PEO coatings. The present paper describes a systematic attempt to investigate the pore content, architecture and scale.

2. Experimental

2.1. Sample preparation

Coatings were produced on 6082 aluminium alloy, in the form of 3 mm thick sheet, with in-plane dimensions of 50 mm \times 50 mm. Coatings were prepared using a 10 kW

* Corresponding author.

E-mail addresses: twc10@cam.ac.uk, twc10@cus.cam.ac.uk (T.W. Clyne).

Keronite processing rig and a standard, commercially available electrolyte, consisting primarily of a dilute aqueous solution of KOH and Na_2SiO_4 . The electrolyte was maintained at a temperature of approximately 25°C by re-circulation through a heat exchanger, with a whistle pump agitating and aerating the electrolyte. A constant capacitance condition was set, so as to achieve a current density of approximately 15 A dm^{-2} after the initial transitory regime. Coatings were grown to a thickness of approximately $100\text{ }\mu\text{m}$. Thicknesses were measured using an Eban 2000 eddy current thickness gauge, the accuracy of which was confirmed by occasional microscopy of cross-sections. Free-standing coatings were obtained by immersion of a coated substrate in a saturated solution of NaOH for several minutes, leading to dissolution of the substrate. Coatings released in this way were then rinsed in water, immersed in concentrated HCl to remove any residual $\text{Al}(\text{OH})_3$ and thoroughly rinsed again in water using an ultrasonic bath. Samples were then dried for several hours at 200°C and allowed to cool before any measurements were performed.

2.2. Microscopy

Scanning electron microscopy (SEM) was used to study the coating microstructure. A typical micrograph of a polished section, obtained using secondary electron mode, is shown in Fig. 1. Image analysis of such sections has been used previously [22] to deduce that typical porosity levels are below 3%. In previous work by the current authors [4], it was pointed out that back-scattered electron mode reveals a more defective structure. An example is shown

in Fig. 2. Back-scattered electrons emerge from an appreciable depth (a few micrometres), so sub-surface features are revealed and polishing artefacts are largely avoided. However, resolution is necessarily lower in this mode, making it hard to resolve fine-scale features. Nevertheless, pipe-like structures appear to be present and these are attributed to the residual cores left by the most recent electrical discharge events. Nevertheless, the overall porosity levels still appear to be relatively low and estimates [4] of the order of 5% have been made.

However, examination of the coating surface at high magnification (using a field emission gun) appears to reveal the presence of extensive, interconnected, fine-scale porosity. This can be seen in Fig. 3, which shows low- and high-magnification images of free surfaces of PEO coatings. The high-magnification image (Fig. 3(b)) shows evidence of a network of fine, surface-connected pores. There is some uncertainty about its origin and nature. For example, substrate dissolution treatments could create pore-like defects in the coating, perhaps by preferentially dissolving amorphous material commonly present in PEO coatings [4]. However, the coating shown in Fig. 3(b) had not been detached from the substrate or exposed to any fluids, etc., so this can be ruled out. Moreover, it is unsurprising that such fine pore structures are not apparent in polished sections, since they are likely to become filled or deformed during preparation.

2.3. Dimensional measurements and weighing in air

A simple approach to porosity estimation is to measure both the dimensions and the mass of a specimen with well-

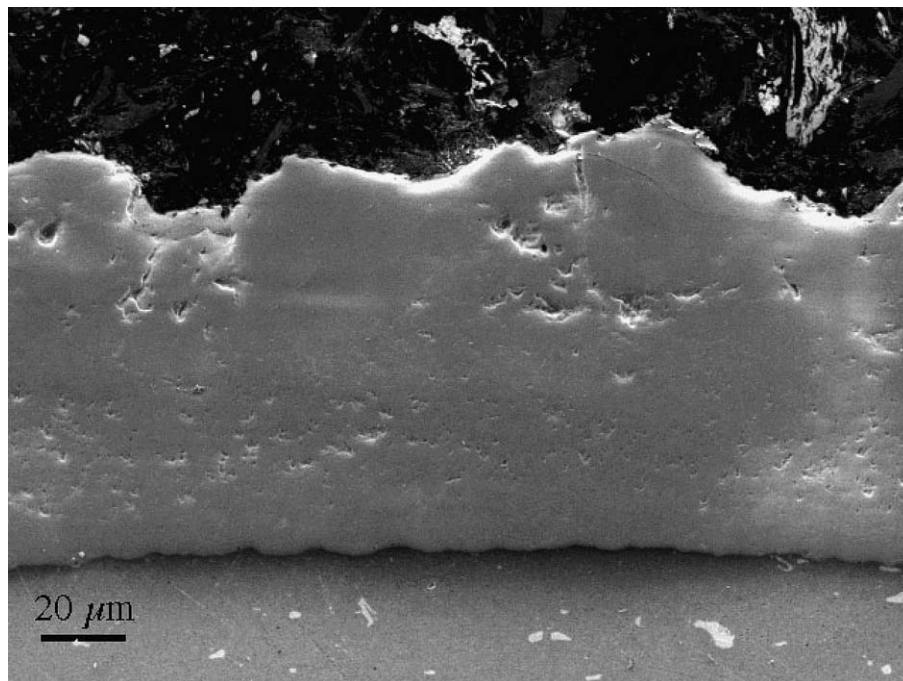


Fig. 1. SEM image (secondary electron mode) of a polished section from a PEO coating on an aluminium alloy substrate, showing little or no obvious porosity.

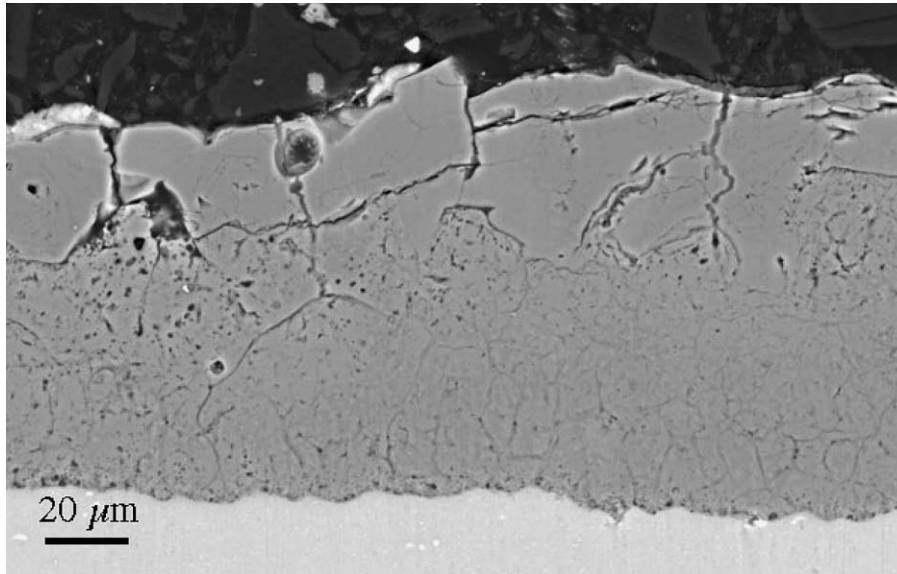


Fig. 2. SEM image (back-scattered electron mode) of a polished section from a PEO coating on an aluminium alloy substrate, showing the fine network of channels created by individual discharge events, apparently representing a porosity level of the order of a few per cent.

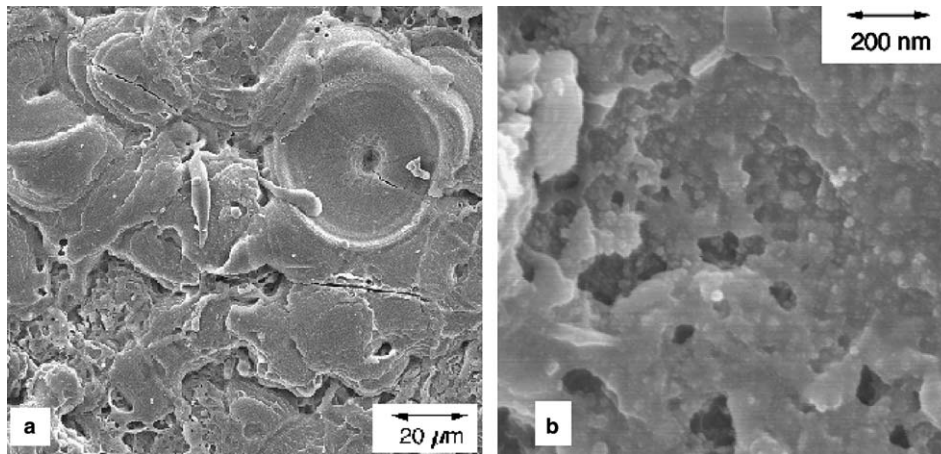


Fig. 3. (a) Low-magnification and (b) high-magnification SEM images (secondary electron mode) of free surfaces of PEO coatings on aluminium alloy substrates.

defined geometry. This gives a bulk density, which can be compared with a theoretical (skeletal) density to estimate the overall porosity. This was done for detached coatings, which were generally in the form of thin plates with linear sides and uniform thickness (measured using the eddy current thickness gauge prior to detaching and with a micrometer after detaching). Weighing was carried out using a Sartorius microbalance with a precision of $\pm 10 \mu\text{g}$. A similar operation was also carried out on attached coatings, with the substrate mass being calculated via its (known) density and measured dimensions and then subtracted from the measured mass of the coated substrate.

2.4. Hydrostatic weighing

Comparison between the weight of free-standing coatings in air and when immersed in a suitable liquid allows

direct measurement of density, without the need for any dimensional assessment of specimen volume. The technique has been described in detail previously [23]. The liquid used in this work was $\text{C}_{11}\text{F}_{20}$ (“Flutec”). This thoroughly wetted the specimens, penetrating any surface-connected porosity. The method therefore provides a measure of skeletal density, assuming that there is no occluded porosity. Corrections must be made for the temperature dependence of the liquid density, and for the buoyancy effect on supporting wires. By coating specimens with lacquer, it is possible to seal the surface-connected porosity and, provided the lacquer density and mass are known, the overall porosity can then be measured. However, due to the fragility of specimens, this was only performed on coatings that were still attached to the substrate, requiring corrections for the presence of the substrate and reducing the precision of the technique.

2.5. Helium pycnometry

Helium pycnometry [24] is another technique giving a measurement of the skeletal density, and hence (by comparison with the theoretical density) an indication of the level of occluded porosity. A MicroMeritics AccuPyc 1330 machine was used. The gas pressure in a calibrated chamber was measured before and after insertion of the specimen into the measurement chamber. The resulting measure of specimen volume was combined with an accurately determined specimen mass to obtain the skeletal density. The system was calibrated before each measurement, using a reference sphere, and each measurement was repeated 50 times, or until the standard deviation of the results was below 0.05%. It was necessary to fill completely a 2 cm³ chamber with free-standing coating material, in order to satisfy the specimen requirements for the instrument.

2.6. Isothermal nitrogen adsorption (BET)

A MicroMeritics TriStar 3000 was used to measure the specific surface area of free-standing coatings. Samples that had been used in the helium pycnometer were re-weighed and dried thoroughly (200 °C overnight) before measurement. The sample chambers were then cooled with liquid N₂ and evacuated. Nitrogen was then introduced in controlled pressure increments, and the equilibrated pressures measured and compared with the saturation pressure, to determine the quantities of adsorbed gas. The Brunauer–Emerett–Teller (BET) adsorption isotherm was then used to determine the specimen surface area.

2.7. Mercury intrusion porosimetry

Mercury intrusion porosimetry [25,26] was used to evaluate the pore size distribution, the pore geometry and the total volume of surface-connected porosity. A MicroMeritics AutoPore IV was used. An accurately weighed mass of sample was placed in a penetrometer, which was evacuated and then back-filled with mercury. Since mercury behaves as a non-wetting liquid (i.e. has a relatively high contact angle), and does not spontaneously penetrate cracks or pores, it must be forced into the specimen by the application of external pressure. The required pressure is inversely proportional to the pore size, in accordance with the Washburn equation for cylindrical pores:

$$P = \frac{-2\gamma \cos \theta}{r}, \quad (1)$$

where P is the applied pressure, γ is the surface tension of the mercury (taken as 0.485 N m⁻¹), θ is the contact angle (taken as 130°) and r is the capillary radius. The penetrometer was progressively pressurised up to 100 MPa, with the penetration volume being monitored by measuring the associated changes in the capacitance of a capillary stem. A pore size distribution was thus obtained, as well as a pore

volume. Estimates of the sample bulk volume and skeletal volume (and hence densities) were also obtained, respectively, from the absolute volumes of penetration at the onset of mercury entry into the coatings and at maximum pressure (full penetration).

3. Porosity content measurement

3.1. Theoretical density

The coating density can in principle be obtained from the proportion of the phases present and their densities. There is some uncertainty about both of these, particularly the density of the amorphous alumina. Measurement of the phase proportions, using X-ray diffraction peak areas, was described in a previous publication [4] and values obtained in that work are employed here. Data are presented in Table 1. The estimated value for the theoretical density is 3.63 (±0.2) g cm⁻³. (The quoted error level is largely associated with uncertainty in the measured phase proportions.) Clearly, the fact that the error level is quite high means that the estimate is of limited utility, but it is at least a reference point worth bearing in mind.

3.2. Bulk (apparent) density

From the measured mass and physical dimensions of free-standing coating fragments, a bulk density of 2.1 (±0.3) g cm⁻³ was obtained. This represents an overall porosity level of 42% (±12%), using the theoretical density estimated in Section 3.1. Similar measurements on attached coatings yielded an even lower bulk density of 1.8 (±0.4) g cm⁻³ and a correspondingly higher porosity level of 50% (±14%). The error levels quoted here are based on scatter in measured data. However, attempting to assess the true error involved in such measurements is fraught with difficulties. In particular, it can be seen in Figs. 1 and 2 that the macroscopic uniformity of the coating thickness is poor. The techniques used to measure the coating thickness will thus tend systematically to overestimate the correct value – this represents an additional effect to the errors quoted above. The above estimates of density are thus likely to be too low and the corresponding porosities too high. All that can really be deduced from these

Table 1
Phase density data from the literature and estimated PEO coating density

Phase	Density (g cm ⁻³)	Source of data	Estimated phase fraction in coating (vol.%)	Calculated density (g cm ⁻³)
α-Al ₂ O ₃	3.987 ± 0.024	[36,37]	35 ± 10	–
γ-Al ₂ O ₃	3.72 ± 0.1	[38]	35 ± 10	–
Amorphous Al ₂ O ₃	3.1 ± 0.1	[39,40]	30 ± 10	–
PEO coating	–	–	–	3.63 ± 0.2

measurements is that there at least appear to be some indications of the presence of substantial porosity.

Mercury porosimetry (Section 4.2) provides an alternative measure of bulk density, based on the un-penetrated volume at low applied pressures. Again, however, substantial uncertainty arises. In this case, it is because flakes of free-standing coating were used, and penetration of the inter-flake spaces requires a certain pressure. Taking the flake surface roughness ($\sim 8 \pm 3 \mu\text{m}$) as a cut-off dimension gave an estimated bulk density of $3.0 (\pm 0.1) \text{ g cm}^{-3}$, as described in Section 4.2. This corresponds to a porosity level of $17\% (\pm 7\%)$. Again, error levels are difficult to estimate, but these data also give clear indications of the presence of substantial porosity.

3.3. Skeletal density

The coating skeletal density was measured using penetrating fluids: $\text{C}_{11}\text{F}_{20}$ liquid in the case of Archimedian density measurements, helium gas in the case of pycnometry and mercury liquid under high pressure in the case of porosimetry (Section 4.4). Results from these test methods are summarised in Table 2, where the quoted uncertainties represent scatter in experimental data. Each technique gives results repeatable to a high consistency and the nominal experimental uncertainty is thus small in all cases. However, it can be seen that there are significant discrepancies between the data obtained by the three methods. Part of this discrepancy may arise from the different depth of surface penetration occurring with each fluid. Mercury is a non-wetting fluid and penetration is only achieved by applying substantial pressure. Since the maximum pressure applied was about 1 kbar, application of Eq. (1) indicates that only pores with diameters greater than 7 nm will be penetrated. The $\text{C}_{11}\text{F}_{20}$ liquid, in contrast, is a strongly wetting fluid, which should penetrate nanometre-scale porosity. This is consistent with the measured (skeletal) density being higher than that obtained from mercury porosimetry. The helium pycnometry, however, gives a relatively low value, which is surprising in view of the expected deep penetration of the helium gas. This may be the result of significant deviation from (assumed) ideal gas behaviour, since the mean free path of helium under ambient conditions is $\sim 1 \mu\text{m}$ and many of the pores are thought to be appreciably finer than this. In any event, it can be seen that all of the measured skeletal density values are quite close to the theoretical coating density ($\sim 3.63 \pm 0.2 \text{ g cm}^{-3}$). This suggests that most of the porosity is

surface-connected, and the level of occluded porosity is very low.

4. Porosity scale, architecture, formation mechanism and consequences

4.1. Specific surface area

Typical BET adsorption isotherm data are shown in Fig. 4. The isotherm plot corresponds to the well-known BET equation

$$\frac{P}{V_a(P_0 - P)} = \frac{1}{V_m C} \left[1 + \frac{P}{P_0} (C - 1) \right], \quad (2)$$

where V_a is the adsorbed volume of gas, V_m is the volume of an adsorbed monolayer of gas, P is the pressure and C is a constant. The gradient and intercept of the plot are used to evaluate V_m and this is in turn used to estimate the specific surface area, S , of the porous material. It can be seen that the data conform well to a linear relationship. The value obtained for S was $4.15 \pm 0.05 \text{ m}^2 \text{ g}^{-1}$. Uncertainties in these data are too small to be indicated on the plot. The quoted error in the final result is based on the conformity of experimental data to a linear fit.

If the pores are taken as arrays of parallel cylinders, then the predicted value of S can be expressed as

$$S = \frac{4p}{d\rho(1-p)}, \quad (3)$$

where p is the pore fraction, ρ is the theoretical (skeletal) density and d is the pore diameter. A plot is shown in Fig. 5 of the value of d indicated by this equation as a function of S for four different porosity levels, using the measured value of S ($4.15 \text{ m}^2 \text{ g}^{-1}$) and the theoretical density (3.63 g cm^{-3}) (see Section 3.1). It can be seen that the measured S is consistent with a (uniform) pore diameter of around 30 nm, assuming a porosity level of 20%.

Table 2
Experimental data for measured skeletal densities of PEO coatings

Method	Measured density (g cm^{-3})
Archimedian weighing	3.73 ± 0.02
Helium pycnometry	3.498 ± 0.004
Mercury porosimetry	3.609 ± 0.004

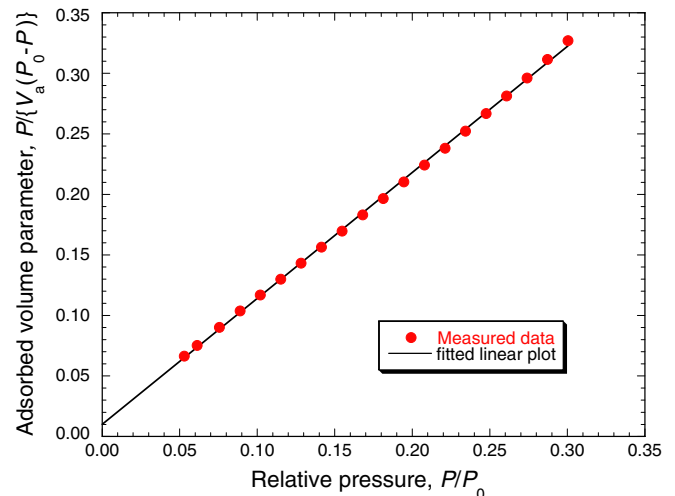


Fig. 4. BET adsorption isotherm for 3.6 g of detached coating.

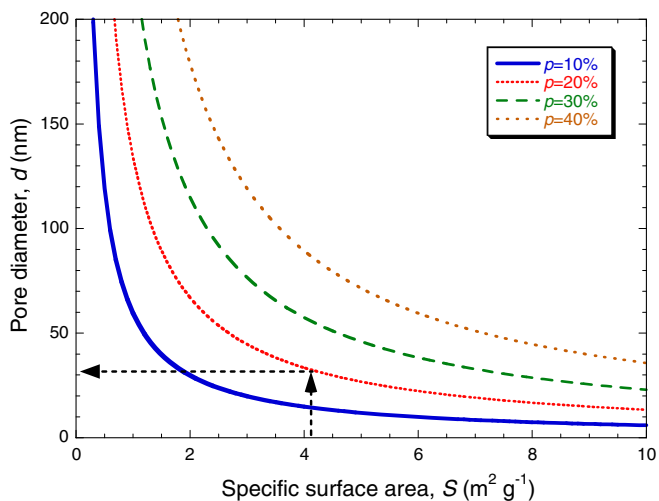


Fig. 5. Plots of pore diameter against specific surface area, S , for different levels of porosity, p . Arrows show how a measured value of S can be used to infer the pore diameter (assumed uniform) for a given porosity content (20% in the example shown).

Significantly, repeated BET measurements performed on a coating still attached to its substrate yielded a similar specific surface area value ($S = 4.0 \pm 0.2 \text{ m}^2 \text{ g}^{-1}$). The error level was substantially increased by the uncertainty in the mass of the substrate, but nevertheless the similarity of the two measured values of S represents clear evidence that the porosity observed in detached coatings was not created during the substrate dissolution procedure.

4.2. Pore size distribution

The distribution of pore size, obtained from mercury intrusion porosimetry, is shown in Fig. 6. The relationship between pressure and pore size is given by Eq. (1). It can be seen in Fig. 6(a) that, by making an assumption about the onset of penetration into the coating interior (based on the surface roughness, as described in Section 3.2), an estimate can be made of the overall porosity level, and of the pore size distribution of this porosity. Since the maximum pressure that could be applied with the equipment concerned was about 100 MPa (~ 1 kbar), penetration is expected only of pores down to about 7 nm in diameter. There are some indications in the shape of the plot that the contribution to the total void content from pores smaller than this may not be entirely negligible, since the incremental pore volume does not fall to zero even at the highest applied pressures. However, by extrapolating the plot to very small pore sizes, it could be deduced that the overall porosity level is about 20%.

In order to check on the probable contributions from very small pores, the gradient of Fig. 6(a) was examined as a function of pore size (pore volume increment) and this parameter was normalised by dividing by the pore size concerned, to give an indication of the population of pores of different sizes. A plot of these parameters is shown in

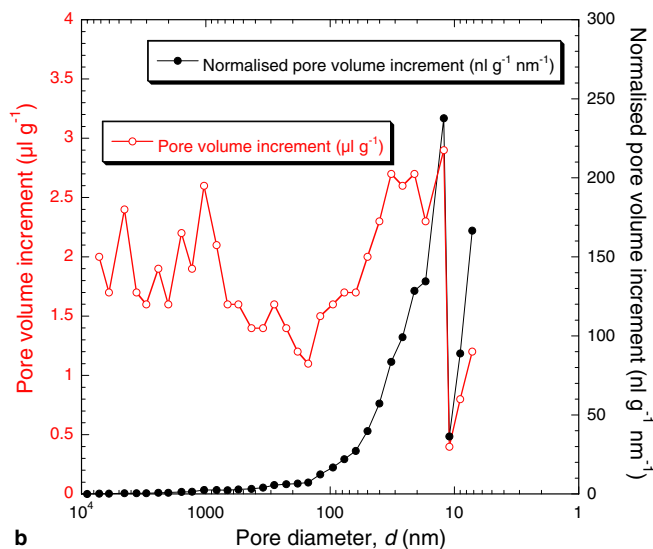
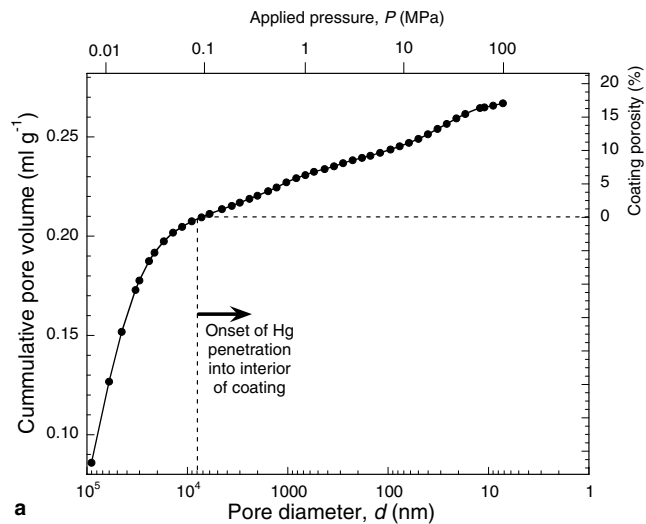


Fig. 6. (a) Cumulative intrusion volume as a function of applied pressure (i.e. pore size), for mercury porosimetry testing on flakes of 100 μm thick PEO coating and (b) the same data plotted as incremental pore volume, with and without normalisation by dividing by the pore diameter.

Fig. 6(b). An approximately bell-shaped plot is expected for the normalised parameter if the data cover the complete range of pore sizes present. It can be seen that the shape of this plot suggests that there probably is some porosity below 7 nm in size, but it is unlikely to be very significant in terms of pore volume.

The pore size distribution shown has been obtained assuming a cylindrical pore geometry. Making this assumption does not affect the deduced pore volume or overall porosity level, but it does affect the distribution of pore size. If, for example, the pore geometry were actually slab-like cracks, then the crack widths would be half the corresponding cylinder diameters. In general, the approximate deduced pore dimensions are not very sensitive to the assumed pore geometry. They will, however, be affected by the presence of “ink-bottle” shaped pores [26]. Whenever pores increase in size, beyond a constriction, the deduced

distribution will be skewed towards finer pore sizes. It has been demonstrated, however, that this is not a great problem for widely interconnected networks [27], although the exact distribution of pore sizes can only be determined by repeated intrusion–extrusion hysteresis measurements over the full range of pressures. Concern has also been expressed [26] that structural damage may be caused by the application of high pressures to porous ceramics, although it is probable that this only becomes a serious problem at very high porosity levels (greater than about 60%).

Finally, from the deduced pore size distribution, again assuming cylindrical pore geometry, the specific surface area can be estimated, using Eq. (3). Applying this equation gives a value for S of about $4.5 \text{ m}^2 \text{ g}^{-1}$. This is slightly larger than that obtained from the BET measurements. Such discrepancies are common [28], and are often due, at least in part, to the ink-bottle effect described earlier, which skews the distribution towards finer pores, raising the surface area. Discrepancies as high as 100% can result from this effect [28]. The fact that the discrepancy is only about 13% in the present case suggests that the ink-bottle effect is not a significant source of error in the application of mercury porosimetry to this material.

4.3. Effects of porosity on coating characteristics

4.3.1. Stiffness

Fine-scale porosity may be partly responsible for the relatively low global stiffness reported recently [4] for these coatings. The MacKenzie relation [29] suggests that 20% porosity is expected to cause a reduction in stiffness of $\sim 30\%$, although it is clear that pore architecture will be relevant to the strength of the effect [30]. In fact, the reported stiffness is about an order of magnitude lower than that of corresponding fully dense material, so there must be defects present other than approximately spherical or cylindrical pores in order to explain the effect. The most likely explanation is the presence of a relatively high concentration of microcracks [31].

4.3.2. Hardness

The hardness is also expected to be sensitive to the presence of porosity. For example, 20% porosity is expected [32] to reduce the hardness from the fully dense value by something like 60–70%. Coupled with the hardening effect of a fine-grain structure, this is broadly consistent with typical measured [4] hardness, which is $\sim 14 \text{ GPa}$ for coatings of the type studied here.

4.3.3. Thermal conductivity

PEO coatings exhibit thermal conductivities approximately an order of magnitude lower than that of bulk alumina [14]. While such low values were initially attributed to the very fine grain size, and the presence of amorphous material, and indeed these features are certainly relevant, the presence of fine porosity would be a further contributory factor. It may be noted that the

fact that the average pore diameter is less than the mean free path of nitrogen or oxygen molecules under ambient conditions will lead to inefficient conduction within the pores. This may partly explain the observation [14] that evacuation had a negligible effect on coating conductivity, although the expected effect would be small in any event.

4.3.4. Permeability

It is perhaps also worth noting that it has been observed previously [33] that X-ray penetration into PEO coatings appears to be deeper than expected. This may be at least partly a consequence of the presence of fine porosity. Furthermore, a major implication of the presence of the proposed porosity structures relates to fluid permeation, impregnation and lubrication, particularly since the porosity appears to be largely interconnected (and surface-connected). It may explain why surface impregnation of PEO coatings with a wide variety of compounds, including paints, sol–gels and polymers, such as Teflon, has proved to be remarkably successful. Furthermore, the observation [34] that friction and wear coefficients are very low with PEO coatings in lubricated systems may be attributable to lubricant penetration and retention in surface-connected pores. These are, of course, beneficial effects. It is also worth noting that adverse effects may arise from fluid permeation, such as penetration of corrosive liquids through the coating, leading to chemical attack of the substrate. It is clear that the wetting characteristics of the liquid will be important. Of course, it should be possible to seal the surface in some way, if it is required that the coating should be impermeable to particular fluids.

4.4. Porosity formation mechanism

The proposed porosity may arise from oxygen evolution during the PEO process, which is commonly blamed for the formation of the more obvious macroscopic pores near PEO coating surfaces. It is certainly worth noting that the high pressures and temperatures are likely to result in significant concentrations of dissolved oxygen in the molten oxides. Because discharges are limited to about $10 \mu\text{s}$ in duration [35], this evolved oxygen is likely to become trapped in molten alumina. It could help create, and escape via, very fine-scale interconnected porosity as the melt is rapidly cooled.

The presence of fine, interconnected porous networks may also help to explain the stable growth of PEO coatings to substantial thicknesses, without prohibitively high dielectric resistance developing and without destructively energetic discharges resulting. The electrolyte would be able to penetrate through the thickness of the coating via such networks, and fine-scale discharges could occur across a relatively thin barrier near the substrate interface. Alternatively, the pores may become gas-filled. This would again provide a lower resistance path. It seems

clear that a detailed process model is required in order to understand fully and optimise PEO coating production, and the presence of a fine porosity network may prove to be significant in this context.

5. Conclusions

The following conclusions can be drawn from this work, relating to PEO coatings on aluminium:

- (a) SEM of polished sections reveals little obvious porosity, although there is evidence from back-scattered images suggesting the presence of pipe-like features and other defects, attributable to the localised electrical discharge events known to occur during coating formation. Estimated porosity levels represented by these structures are of the order of a few per cent. However, high-magnification (SEM using a field emission gun) study of coating surfaces suggests the presence of an extensive network of much finer (sub-micrometre) porosity.
- (b) The bulk density of PEO coatings on aluminium has been measured at about 3 g cm^{-3} . This is significantly lower than the skeletal density, which has been measured to be about 3.7 g cm^{-3} , or the theoretical density obtained from individual phase densities, which is also about 3.7 g cm^{-3} . This suggests that the coatings are approximately 20% porous and that this porosity is largely surface-connected – i.e. there is little or no occluded porosity.
- (c) The size distribution of this porosity has been studied by BET adsorption and mercury porosimetry experiments. It is concluded from these studies that the average pore size is of the order of 30 nm and that most of the pores fall in the size range 5 nm–1 μm . Data from these investigations are also consistent with an overall porosity level of around 20%.
- (d) This porosity is expected to influence various properties and characteristics. For example, it may at least partially account for the observed high capacity for liquid impregnation, the low stiffness, the low thermal conductivity and the low friction and good wear resistance under lubricating conditions. Most of these property changes are decidedly beneficial. For example, a reduced stiffness limits the differential thermal expansion stresses and a low conductivity favours effective thermal barrier function. An adverse effect is expected on the coating hardness, but this is not a large effect and in general the coatings are relatively strong.
- (e) The porosity may form as a consequence of oxygen entrapment in molten alumina in the vicinity of localised electrical discharges, which occur during PEO coating formation. It is possible that the pore network facilitates the formation of relatively thick coatings, by allowing electrolyte to penetrate deep into the growing layer during the process.

Acknowledgements

Financial support for the work described in this article has come from EPSRC and DSTL. There has also been extensive collaboration with Keronite Ltd. The authors are grateful to Dr. Igor Golosnoy (Materials Science Department, Cambridge University), Prof. Richard Jones (DSTL) and Steve Hutchins (Keronite) for helpful discussions.

References

- [1] Yerokhin AL, Nie X, Leyland A, Matthews A, Dowey SJ. *Surf Coat Technol* 1999;122:73–93.
- [2] Nie X, Leyland A, Song HW, Yerokhin AL, Dowey SJ, Matthews A. *Surf Coat Technol* 1999;119:1055–60.
- [3] Gnednikov SV, Khrisanfova OA, Zavidnaya AG, Sinebrukhov SL, Gordienko PS, Iwatsubo S, et al. *Surf Coat Technol* 2001;145:146–51.
- [4] Curran JA, Clyne TW. *Surf Coat Technol* 2005;199:168–76.
- [5] Voevodin AA, Yerokhin AL, Lyubimov VV, Donley MS, Zabinski JS. *Surf Coat Technol* 1996;86–87:516–21.
- [6] Tian J, Luo ZZ, Qi SK, Sun XJ. *Surf Coat Technol* 2002;154:1–7.
- [7] Nie X, Meletis EI, Jiang JC, Leyland A, Yerokhin AL, Matthews A. *Surf Coat Technol* 2002;149:245–51.
- [8] Rama-Krishna L, Somaraju KRC, Sundararajan G. *Surf Coat Technol* 2003;163–164:484–90.
- [9] Barik R, Wharton JA, Wood RJK, Stokes KR, Jones RL. In: Sedriks J, Agarwala V, Mantz R, Beatty J, editors. *Tri-service corrosion conference*. Chester, PA: Navmar Applied Science; 2003.
- [10] Wei T, Yan F, Tian J. *J Alloys Compd* 2004;389:169–76.
- [11] Yerokhin AL, Nie X, Leyland A, Matthews A. *Surf Coat Technol* 2000;130:195–206.
- [12] Butyagin PI, Khokhryakov YV, Mamaev AI. *Mater Lett* 2003;57:1748–51.
- [13] Gnednikov SV, Khrisanfova OA, Zavidnaya AG, Sinebrukhov SL, Kovryanov AN, Scorobogatova TM, et al. *Surf Coat Technol* 2000;123:24–8.
- [14] Curran JA, Clyne TW. *Surf Coat Technol* 2005;199:177–83.
- [15] Yerokhin AL, Voevodin AA, Lyubimov VV, Zabinski J, Donley M. *Surf Coat Technol* 1998;110:140–6.
- [16] Yerokhin AL, Leyland A, Matthews A. *Appl Surf Sci* 2002;200:172–84.
- [17] Sundararajan G, Krishna LR. *Surf Coat Technol* 2003;167:269–77.
- [18] Guangliang Y, Xianyi L, Yizhen B, Haifeng C, Zengsun J. *J Alloys Compd* 2002;345:196–200.
- [19] Xue WB, Deng ZW, Chen RZ, Zhang TH, Ma H. *Surf Coat Technol* 2001;36:2615–9.
- [20] Xue WB, Wang C, Chen RY, Deng ZW. *Mater Lett* 2002;52:435–41.
- [21] Han Y, Hong SH, Xu KW. *Surf Coat Technol* 2003;168:249–58.
- [22] Shrestha S, Merstlinger A, Sickert D, Dunn BD. In: *Proceedings of the ninth international symposium on materials in a space environment*; 2003. pp. 57–65.
- [23] Whitehouse AF, Warwick CM, Clyne TW. *J Mater Sci* 1991;26:6176–82.
- [24] Petropoulos JH, Tsimillis K, Savvakis C, Havredaki V. *J Phys E Sci Instrum* 1983;16:1112–5.
- [25] Van Brakel J, Modry S, Svata M. *Powder Technol* 1981;29:1–12.
- [26] Moscou L, Lub S. *Powder Technol* 1981;29:45–52.
- [27] Wardlaw NC, McKellar M. *Powder Technol* 1981;29:127–43.
- [28] Dees PJ, Polderman J. *Powder Technol* 1981;29:187–97.
- [29] MacKenzie JK. *Proc Phys Soc* 1950;B63:2–11.
- [30] Markaki AE, Colombo P, Clyne TW. In: Bassani F, Liedl GJ, Wyder P, editors. *Encyclopedia of condensed matter physics*. Oxford: Elsevier; 2005. p. 318–32.

- [31] Kroupa F, Dubsy J. *Scripta Mater* 1999;40:1249–54.
- [32] McColm IJ. *Ceramic hardness*. New York, NY: Plenum Press; 1990.
- [33] Xue WB, Deng ZW, Lai YC, Chen RY. *J Am Ceram Soc* 1998;81:1365–8.
- [34] Dearnley PA, Gummersbach J, Weiss H, Ogwu AA, Davies TJ. *Wear* 1999;225:127–34.
- [35] Van TB, Brown SD, Wirtz GP. *ACS Bull* 1977;56:563–6.
- [36] Kelly A, Groves GW. *Crystallography and crystal defects*. Herndon, VA: TechBooks, Longman Group; 1970.
- [37] Huang T. *Adv X-ray Anal* 1990;33:295.
- [38] Liddell K. *JCPDS-International Centre for Diffraction Data* 1996 2001 [cited: PCPDFWIN file number 50-0741].
- [39] Alcalá G, Skeldon P, Thompson GE, Mann AB, Habazaki H, Shimizu K. *Nanotechnology* 2002;13:451–5.
- [40] Proost J, Spaepen F. *J Appl Phys* 2002;91:204–16.